A High-Fat Diet Attenuates AMPK α1 in Adipocytes to Induce Exosome Shedding and Nonalcoholic Fatty Liver Development In Vivo

Chenghui Yan,[1,2] Xiaoxiang Tian,[2] Jiayin Li,[2,3] Dan Liu,[2] Ding Ye,[1] Zhonglin Xie,[1] Yaling Han,[2] and Ming-Hui Zou[1]

Diabetes 2021;70:577–588 | https://doi.org/10.2337/db20-0146

Exosomes are important for intercellular communication, but the role of exosomes in the communication between adipose tissue (AT) and the liver remains unknown. The aim of this study is to determine the contribution of AT-derived exosomes in nonalcoholic fatty liver disease (NAFLD). Exosome components, liver fat content, and liver function were monitored in AT in mice fed a high-fat diet (HFD) or treated with metformin or GW4869 and with AMPKα1-floxed (*Prkaα1*$^{fl/fl}$/wild-type [WT]), *Prkaα1*$^{-/-}$, liver tissue-specific *Prkaα1*$^{-/-}$, or AT-specific *Prkaα1*$^{-/-}$ modification. In cultured adipocytes and white AT, the absence of *AMPKα1* increased exosome release and exosomal proteins by elevating tumor susceptibility gene 101 (*TSG101*)–mediated exosome biogenesis. In adipocytes treated with palmitic acid, TSG101 facilitated scavenger receptor class B (CD36) sorting into exosomes. CD36-containing exosomes were then endocytosed by hepatocytes to induce lipid accumulation and inflammation. Consistently, an HFD induced more severe lipid accumulation and cell death in *Prkaα1*$^{-/-}$ and AT-specific *Prkaα1*$^{-/-}$ mice than in WT and liver-specific *Prkaα1*$^{-/-}$ mice. AMPK activation by metformin reduced adipocyte-mediated exosome release and mitigated fatty liver development in WT and liver-specific *Prkaα1*$^{-/-}$ mice. Moreover, administration of the exosome inhibitor GW4869 blocked exosome secretion and alleviated HFD-induced fatty livers in *Prkaα1*$^{-/-}$ and adipocyte-specific *Prkaα1*$^{-/-}$ mice. We conclude that HFD-mediated AMPKα1 inhibition promotes NAFLD by increasing numbers of AT CD36-containing exosomes.

Exosomes are nanosized biovesicles (30–100 nm) secreted by cells, and they contain miRNAs, mRNAs, and proteins from parent cells (1). When internalized by recipient cells, exosomes exert regulatory effects by delivering their internal bioactive components (2). Increasing evidence indicates that exosomes play important roles in intercellular communications, including the immune response (3), tumor progression (4), and cell metabolism (5). Understanding the molecular mechanisms by which exosome biogenesis and heterogeneity are regulated by cells, including the cargo components and secretion, is a major challenge.

Adipose tissue (AT) is an important endocrine organ that has a central role regulating energy metabolism (6,7). Obesity-induced AT damage and ectopic deposition are the primary pathological factors that lead to insulin resistance, diabetes, and a nonalcoholic fatty liver (NAFL) (8–10). Notably, AT is a major source of exosomes. For example, exosome secretion is observed in cultured AT (11,12) and adipocytes (13). In addition, obesity significantly increases exosome secretion from AT in vivo (14). In contrast, specific stimuli that are associated with a reduction in body weight, such as starvation and rapamycin, significantly reduce exosome secretion (15,16). These results strongly suggest that AT is a major source of circulating exosomes and that body weight dynamics modulate circulating exosome levels. Because obesity is closely associated with the development of metabolic disorders, including NAFL disease (NAFLD), it is imperative that the role of AT-derived exosomes in the development of a NAFL is identified.

[1]Center for Molecular and Translational Medicine, Georgia State University, Atlanta, GA
[2]Cardiovascular Research Institute and Department of Cardiology, General Hospital of Northern Theater Command, Shenyang, China
[3]College of Life and Health Sciences, Northeastern University, Shenyang, China
Corresponding author: Chenghui Yan, yanch1029@163.com, or Yaling Han, hanyaling@263.net

Received 12 February 2020 and accepted 19 November 2020

This article contains supplementary material online at https://doi.org/10.2337/figshare.13259768.

AMPK is a ubiquitous energy-sensing enzyme within cells (17–19) that is critical to maintaining metabolic homeostasis. AMPK activation is thought to mediate the beneficial effects of metformin, the most widely used antidiabetic drug worldwide (20,21). Intriguingly, reduced AMPK activity in white AT (WAT) occurs in obese animals and humans (22). The effect of attenuated AMPK activity on exosome biogenesis, cargo contents, and shedding in WAT remains unknown. In this study, we report that AMPKα1 activation in WAT mitigates high-fat diet (HFD)–induced NAFL by ablating exosome biogenesis and secretion.

RESEARCH DESIGN AND METHODS

Cell Culture and Induction of Adipocyte Differentiation

The mouse preadipocyte cell line 3T3L1 and HepG2 cells were cultured in high-glucose Dulbecco's minimal essential medium with 10% exosome-depleted FBS (System Biosciences, Palo Alto, CA), 1% Glutamax (Invitrogen, Carlsbad, CA), 1% nonessential amino acids (Invitrogen), 1% sodium pyruvate (Invitrogen), and 1% penicillin/streptomycin (Gibco, Grand Island, NY). Cultured cells were incubated at 37°C in a humidified atmosphere of 5% CO_2 and 95% air. 3T3L1 cell differentiation was carried out as described previously (23). Briefly, 3T3L1 cells were cultured in preadipocyte differentiation medium (ScienCell Research Laboratories, Carlsbad, CA) for 7–10 days to induce their differentiation into mature adipocytes.

Palmitic Acid Preparation and Treatments

Differentiated 3T3L1 adipocytes were treated with palmitic acid (PA) (0.3 mmol/L) dissolved in 0.5% albumin (Sigma-Aldrich, St. Louis, MO) for 12 or 24 h. To induce endocytosis or lipid accumulation, HepG2 cells were treated with exosomes with or without PA.

Exosome Isolation and Counting

Media were collected after culturing of cells or AT under the designated conditions. Exosomes were extracted with Total Exosome Isolation Kits (Thermo Fisher Scientific, Waltham, MA) according to the manufacturer's instructions. Exosome pellets were suspended in PBS. To quantify isolated exosomes, acetylcholinesterase activity assays were performed using the EXOCET system (System Biosciences). To characterize exosomes, the isolated preparations were analyzed with a dynamic light-scattering system (Zetasizer Nano; Malvern Panalytical, Malvern, U.K.) and transmission electron microscopy (TEM).

Western Blotting and Immunoprecipitation

Cell or AT exosome protein were extracted using radioimmunoprecipitation assay buffer (sc-24948; Santa Cruz Biotechnology, Dallas, TX) and quantified using the BCA protein assay (#23225; Pierce Biotechnology, Rockford, IL). Immunoprecipitates and cell or exosome lysates were subjected to Western blotting with specific primary antibodies (Supplementary Table 1) followed by detection with horseradish peroxidase–conjugated secondary antibodies and enhanced chemiluminescence.

Histology and Immunohistochemistry

Liver tissue sections or HepG2 cells were stained with hematoxylin and eosin (H&E) or Oil Red O to quantify the lesion sizes. For immunostaining, HepG2 cells were incubated first with cleaved caspase-3 antibodies (Cell Signaling Technology, Danvers, MA) and subsequently with fluorochrome-conjugated secondary antibodies.

Proteomic Profiling Mass Spectrometry System

Samples were dissolved in lysis buffer composed of 7 mol/L urea (Bio-Rad Laboratories, Hercules, CA), 2 mol/L thiourea (Sigma-Aldrich), and 0.1% 3-cholamidopropyl dimethylammonio 1-propanesulfonate (Bio-Rad Laboratories). Then, the tissues were ground with three TiO_2 abrasive beads (70 Hz for 120 s) followed by centrifugation at 5,000*g* for 5 min at 4°C. The supernatant was collected and centrifuged at 15,000*g* for 30 min at 4°C. The final supernatants were collected and stored at −80°C until use. Desalted peptides were labeled with iTRAQ reagents (iTRAQ Reagent-8PLEX Multiplex Kit; Sigma-Aldrich) according to the manufacturer's instructions. Briefly, the iTRAQ-labeled peptide mix was fractionated using a C18 column (Waters BEH C18 4.6 × 250 mm, 5 μm; Waters Corporation, Milford, MA) on a Rigol L3000 HPLC system (Rigol, Beijing, China) operating at 1 mL/min with a column oven set at 50°C. Mobile phases A (2% acetonitrile [ACN], pH adjusted to 10.0 using NH_4OH) and B (98% ACN, pH adjusted to 10.0 using NH_4OH) were used to develop a gradient elution. The acquired peptide fractions were suspended with 20 μL buffer A (0.1% formic acid and 2% ACN) and centrifuged at 14,000*g* for 10 min. Next, 10 μL of the supernatants were injected into the nano-ultrahigh-performance liquid chromatography tandem mass spectrometry (MS) system consisting of a Nanoflow HPLC system (EASY-nLC 1000) and Orbitrap Fusion Lumos MS (Thermo Fisher Scientific). Identification parameters were set as follows: precursor ion mass tolerance, ±15 ppm; fragment ion mass tolerance, ±20 mmu; maximum missed cleavages, 2; static modification, carboxyamidomethylation (57.021 Da) of Cys residues; and dynamic modifications, oxidation modification (+15.995 Da) of Met residues. Primary data with a P value ≤0.05 and a difference ratio ≥1.2 were selected for further analysis.

Quantitative Real-time PCR

Total RNA was extracted from cells or AT with an RNeasy Mini Kit (#74106; Qiagen, Hilden, Germany) and reverse transcribed with an iScript cDNA synthesis kit (#170-8891; Bio-Rad Laboratories). Real-time PCR was performed with the CFX96 Real-Time System (Bio-Rad Laboratories). The primer sequences used for amplifying mouse genes were as follows: Gapdh forward, 5′-CTA C CCC ACG GCA AGT TCA-3′ and reverse, 5′-CCA GTA GAC TCC ACG ACA AC-3′; tumor susceptibility gene 101 (Tsg101) forward,

5′-CCA TCC CCT CTA GTG CTC GTC-3′ and reverse, 5′-TGC GGA AGA GTC GGT AGT CT-3′; Cd63 forward, 5′-TCA TCC AAA CGT GTA TCC TTC TG-3′ and reverse, 5′-CTT GTG CTC GGA CCC TTT TCT-3′; and Cd36 forward, 5′-TGA TTA ACG GGA CAG ACG GAG AC-3′ and reverse, 5′-ACG TTC TCA AAG CTG CTG AAA GTG-3′.

Gene Silencing

siRNAs targeting mouse *Prkaα1* (sc-29647), *Prkaα2* (sc-38924), *Cd63* (sc-35792), *Tsg101* (sc-36753), and *Cd36* (sc-37245) were purchased from Santa Cruz Biotechnology. Mouse 3T3L1 cells were transfected with 10 μmol/L siRNA using Lipofectamine RNAiMAX (13778150; Life Technologies, Carlsbad, CA) according to the manufacturer's instructions.

Generation of Hepatocyte- or Adipocyte-Specific Prkaα1 Knockout Mice

$Prkaα1^{-/-}$ and $Prkaα2^{-/-}$ mice were generated as previously described (24,25). $Prkaα1^{fl/fl}$ mice were provided by Dr. Benoit Viollet. Hepatocyte- or adipocyte-specific *Prkaα1* knockout mice were generated by crossing $Prkaα1^{fl/fl}$ mice with Alb^{Cre} *or* $Adiponectin^{Cre}$ ($Adipo^{Cre}$) transgenic mice. The mice were fed an HFD (60% kcal fat from lard; D12492; Research Diets, New Brunswick, NJ) or a normal diet, followed by collection of WAT or liver tissue. Animal studies were approved by the Institutional Animal Care and Use Committee at Georgia State University. Serum cholesterol and triglyceride levels were measured using Infinity reagents from Thermo Fisher Scientific according to the manufacturer's instructions (26).

Statistical Analyses

Data obtained were analyzed using SPSS version 24.0 (IBM Corporation, Armonk, NY) and are presented as mean ± SEM. Statistical differences were analyzed by one-way ANOVA followed by Tukey post hoc test. Differences were considered significant at $P < 0.05$.

Data and Resource Availability

The data sets generated during and/or analyzed during the current study are available from the corresponding author upon reasonable request.

RESULTS

Inactivation of AMPK Increases Exosome Secretion in Adipocytes

To elucidate the relationship between AMPKα and exosome secretion in adipocytes, adipocytes were treated with either the AMPK activator AICAR (1 mmol/L) or the AMPK inhibitor compound C (CC; 50 μmol/L) (27) for 6–24 h. Exosomes were then isolated and purified. TEM and diameter analyses revealed approximately spherical vesicles (Supplementary Fig. 1*A*) that had diameters of 40–200 nm (Supplementary Fig. 1*B*). Consistent with an earlier report of adipocytes (27), Western blotting showed that adipocyte treatment with AICAR for 6 h significantly increased AMPK phosphorylation at Thr172. AMPK activation was associated with a significant reduction in exosome number (Fig. 1*A* and Supplementary Fig. 1*B*). In contrast, CC dramatically reduced AMPKα phosphorylation (Supplementary Fig. 1*C* and *D*) and simultaneously increased exosomes in adipocytes (Fig. 1*A* and Supplementary Fig. 1*B*).

CD81 and CD63 are the two major exosome marker proteins, and their expression in exosomes can be used to quantify exosome secretion by cells or tissues (28,29). We next investigated the effect of altered AMPK activity on CD81 and CD63 levels in adipocyte-derived exosomes. Inhibition of AMPK by CC treatment significantly increased CD81 and CD63 levels in exosomes (Fig. 1*B–D*). Conversely, activation of AMPK by AICAR significantly decreased CD81 and CD63 levels in exosomes (Fig. 1*B–D*). These results suggest that AMPK activity negatively regulates exosome secretion in adipocytes.

Silencing of AMPKα1, But Not AMPKα2, Increases Exosome Secretion in Cultured Adipocytes

Noting that AMPK has two catalytic isoforms, AMPKα1 and α2 (25), we next identified the AMPKα isoform that regulates exosome secretion in adipocytes. Adipocytes were transfected with si*Prkaa1* (*Prkaα1* siRNA) or si*Prkaα2*-(*Prkaα2* siRNA). Silencing of *Prkaα1*, but not *Prkaα2*, dramatically increased exosome secretion in adipocytes (Fig. 1*F–H*). Consistent with this finding, *Prkaα1* silencing caused a robust increase in CD63 and CD81 levels in adipocyte-derived exosomes (Fig. 1*F–H*). *Prkaα2* silencing had no effect on CD63 and CD81 levels in the exosomes (Fig. 1*E–H*).

Deletion of AMPKα1 Enhances Exosome Release From Cultured WAT

We further verified that AMPKα1 inactivation increased exosome release ex vivo by collecting exosomes from the medium of cultured wild-type (WT; C57BL/6J), *Prkaα1*-knockout ($Prkaα1^{-/-}$), and *Prkaα2*-knockout ($Prkaα2^{-/-}$) mouse WATs. Similar to the findings with cultured adipocytes, $Prkaα1^{-/-}$ WAT shed more exosomes (Fig. 1*I*) and had higher levels of exosomal CD63 and CD81 proteins (Fig. 1*J–L*) when compared with WT WAT. Deletion of *Prkaα2* had no effect on exosome number or exosomal CD63 and CD81 levels (Fig. 1*J–L*). Taken together, our results indicate that AMPKα1, but not AMPKα2, inhibits exosome secretion in adipocytes.

AMPKα1 Deficiency Enhances Exosome Release Independently of CD63

There are two pathways that regulate exosome secretion: the endosomal sorting complexes required for transport (ESCRT)–dependent and ESCRT-independent pathways (30,31). To determine the mechanism by which AMPK regulates exosome release, we first quantified CD63 expression in adipocytes treated with AICAR (1 mmol/L) or CC (50 μmol/L). AICAR treatment significantly increased CD63 protein levels. Conversely, CC treatment decreased CD63 protein level in adipocytes (Supplementary Fig. 2*A* and *B*). However, neither AICAR nor CC altered CD63 mRNA expression in adipocytes (Supplementary Fig. 2*C*). Similarly, *Prkaα1* silencing reduced CD63 protein levels

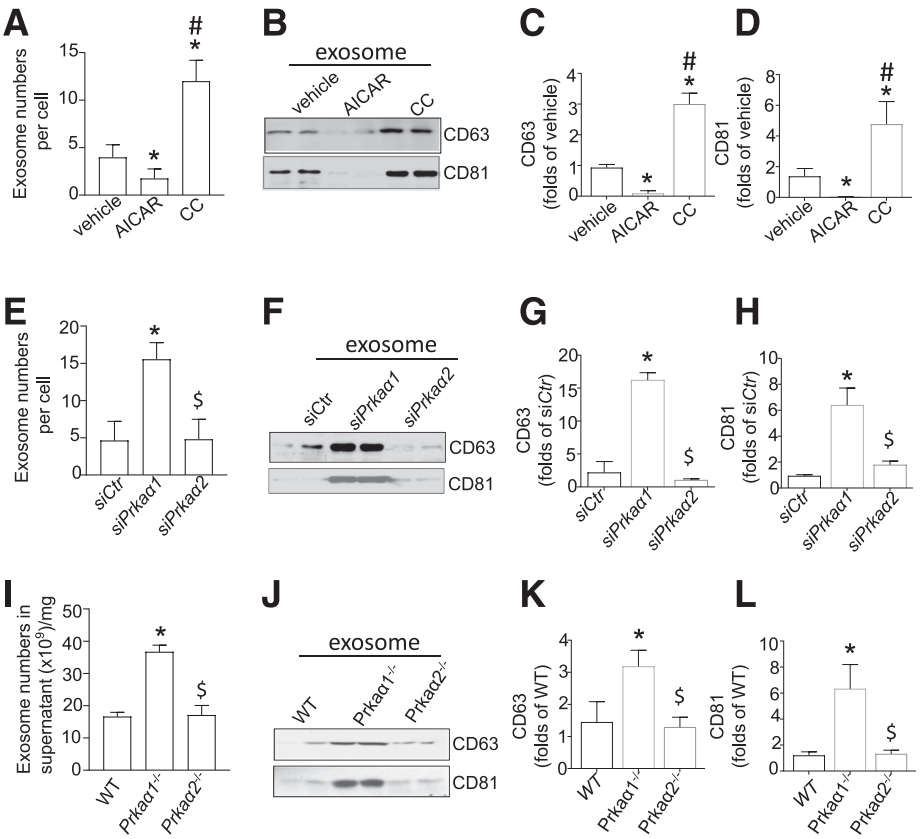

Figure 1— AMPKα1 inhibition enhances exosome release from adipocytes and WAT. *A*: The exosomes internalized by adipocytes that were treated with AICAR (1 mmol/L) or CC (50 nmol/L) were counted using the EXOCET Kit. *B*: Samples with equal amounts of exosomes were analyzed for CD63 and CD81 with Western blotting. *C* and *D*: Densitometric analysis of the Western blots from *B*. *E*: Quantification of exosomes in the medium of 3T3L1-derived adipocytes that were transfected with si*Prkaα1* or si*Prkaα2*. *F*: Samples with equal amounts of exosomes were analyzed for CD63 and CD81 by Western blotting. *G* and *H*: Densitometric analysis of the Western blots from *F*. *I*: Quantification of exosomes in WAT in WT, *Prkaα1*$^{-/-}$, and *Prkaα2*$^{-/-}$ mice ($n = 5$). *J*: Samples with equal amounts of exosomes were analyzed for CD63 and CD81 by Western blotting. *K* and *L*: Densitometric analysis of the Western blots from *J*. *$P < 0.05$ vs. control ($n = 3$); #$P < 0.05$ vs. control group treated with AICAR treatment; \$$P < 0.05$ vs. control group treated with siPrkaα1$^{-/-}$ or Prkaα1$^{-/-}$ group ($n = 3$).

(Supplementary Fig. 2*D* and *E*), but had no effect on CD63 mRNA expression (Supplementary Fig. 2*F*). To determine whether reduced CD63 mediated AMPKα1 deficiency–enhanced exosome secretion, adipocytes were treated with the ceramide-induced exosome inhibitor GW4869 (32). GW4869 enhanced CD63 protein levels (Supplementary Fig. 2*H* and *I*) and reduced exosome secretion in a dose-dependent manner (Supplementary Fig. 2*G*).

To further investigate the effects of reduced CD63 on AMPKα1 deficiency–enhanced exosome secretion, adipocytes that underwent CD63 siRNA transfection were treated with CC to inhibit AMPK activity. *Cd63* silencing did not alter exosome numbers in cells transfected with control siRNA and did not prevent CC-enhanced exosome numbers in adipocytes (Supplementary Fig. 2*J*). These results suggest that AMPKα1 inhibition or silencing increases adipocyte exosome secretion independently of CD63.

AMPKα1 Deficiency Enhances Exosome Biogenesis by Upregulating TSG101

TSG101 is a core component of the ESCRT pathway and plays an important role in the biogenesis of multivesicular bodies (MVBs) (33). Therefore, we investigated whether TSG101 was required for AMPKα1-regulated exosome release. To this end, we first studied the effect of TSG101 on AMPKα1 expression. AICAR significantly reduced TSG101 protein levels, and CC markedly enhanced TSG101 protein levels (Fig. 2*A* and *B*). Neither AICAR nor CC affected TSG101 mRNA expression (Supplementary Fig. 3*A*).

Next, we tested if AMPKα1 directly regulated TSG101 expression by transfecting 3T3L1-derived adipocytes with control siRNA or *Prkaα1* siRNA (si*Prkaα1*). Silencing *Prkaα1*, but not *Prkaα2*, robustly increased TSG101 protein levels (Fig. 2*C* and *D*). Neither si*Prkaα1* nor si*Prkaα2* affected TSG101 mRNA expression (Supplementary Fig. 3*B*).

To validate the results with cultured adipocytes, we measured TSG101 expression in cultured WATs from WT, *Prkaα1*$^{-/-}$, and *Prkaα2*$^{-/-}$ mice. Consistent with the prior data, TSG101 levels in *Prkaα1*$^{-/-}$ WAT were significantly higher than TSG101 levels in either WT or *Prkaα2*$^{-/-}$ WATs (Fig. 2*E* and *F*).

Next, we investigated if increased TSG101 protein was required for AMPKα1-mediated exosome release. Our data indicated that *Tsg101* silencing in adipocytes (Supplementary

Fig. 4) abolished CC-enhanced exosome secretion (Fig. 2*G*) and elevated levels of the exosomal proteins CD63 and CD81 (Fig. 2*H–J*). Furthermore, TEM revealed that the number of MVBs in si*Prkaα1*-treated adipocytes was significantly higher when compared with si*Control* (si*Ctr*)–treated cells. Silencing both *Tsg101* and *Prkaα1* dramatically reduced the biogenesis of MVBs (Fig. 2*K*). Taken together, TSG101 is required for AMPKα1 inhibition–induced exosome formation and exosomal protein expression in adipocytes.

PA Increases Exosome Release by Inhibiting AMPKα1

Obesity increases exosome secretion from WAT (12,13), and PA suppresses AMPK activity in WAT. We hypothesized that PA promotes exosome secretion from WAT via AMPK inhibition. To test this hypothesis, we treated adipocytes with AICAR (1 mmol/L) for 4 h, followed by treatment with PA (300 μmol/L) for 24 h. We next analyzed exosome secretion and found that PA treatment dramatically increased exosome secretion associated with low levels of phosphorylated AMPKα (Supplementary Fig. 5*A–C*). Further, PA-induced exosome increase was abolished by AICAR treatment (Supplementary Fig. 5*A–C*).

Next, we determined if *Prkaα1* overexpression inhibited PA-enhanced exosome secretion. Overexpression of the adenovirus encoding for *Prkaα1* almost completely prevented PA-enhanced exosome secretion (Supplementary Fig. 5*D*). We further examined if AMPKα1 inhibition blocked the effect of AICAR on PA-enhanced exosome secretion. AICAR treatment abolished PA-increased exosome secretion in WT WATs and *Prkaα2*$^{-/-}$ WATs but had no effect on *Prkaα1*$^{-/-}$ WATs (Supplementary Fig. 5*E*). Moreover, the increase of exosomal proteins CD63 and CD81 induced by PA was also inhibited by AICAR treatment (Supplementary Fig. 5*F* and *G*). These results suggest that PA increases exosome release by inhibiting AMPKα1.

PA-Treated Exosomes Released From AMPKα1-Deficient Adipocytes Exacerbate Hepatocyte Damage

To understand the contribution of WAT-derived exosomes to liver damage, we investigated the response of cultured hepatocytes to exosomes derived from PA-treated adipocytes.

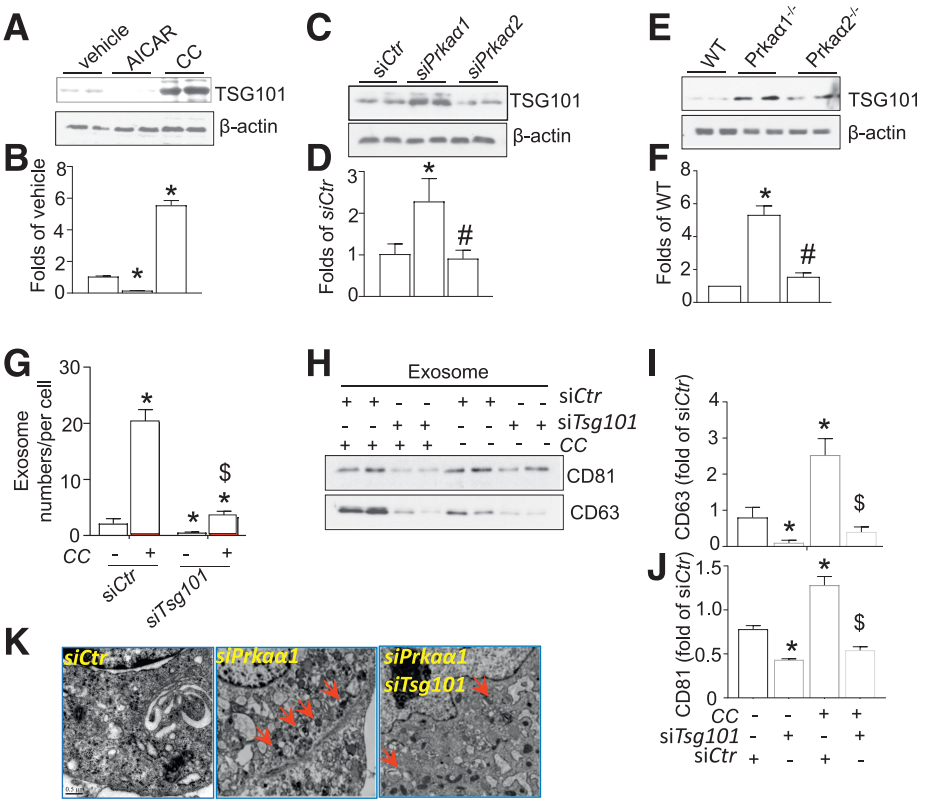

Figure 2—AMPKα1 deficiency enhances exosome biogenesis by upregulating TSG101. *A*: Western blot for TSG101 in adipocytes treated with AICAR or CC. *B*: Densitometric analysis of TSG101 Western blots from *A*. *C*: Western blot for TSG101 in adipocytes transfected with siCtr, *siPrkaα1*, and *siPrkaα2* siRNA. *D*: Densitometric analysis of TSG101 Western blots from *B*. *E*: Western blot for TSG101 in WT, *Prkaα1*$^{-/-}$, and *Prkaα2*$^{-/-}$ adipocytes. *F*: Densitometric analysis of TSG101 Western blots from *E*. *G*: Quantification of exosomes in the medium from adipocytes transfected with si*Tsg101* and treated with or without *CC*. *H*: Western blot for CD63 and CD81 in exosomes derived from adipocytes transfected with si*Tsg101* and treated with or without *CC*. *I* and *J*: Densitometric analysis of CD63 and CD81 Western blots from *H*. *K*: Representative TEM images of MVBs in adipocytes that were transfected with *siPrkaa1 or siTsg101* siRNA and treated with or without CC. Red arrows indicate MVBs. Scale bar = 0.5 μm. *$P < 0.05$ vs. control; #$P < 0.05$ vs. *siPkraα1* or Prkaα1$^{-/-}$ group; \$$P < 0.05$ vs. *CC*-treated *siCtr* group ($n = 3$).

HepG2 cells were treated with equal amounts of exosomes isolated from si*Ctr*- or si*Prkaα*-transfected adipocytes that were pretreated with or without PA. Interestingly, exosome uptake by HepG2 cells was nonuniform. HepG2 cells favored exosomes that were derived from si*Prkaα1*-transfected adipocytes pretreated with PA (Fig. 3*A* and *B*). Oil Red O staining indicated that lipid accumulation was exacerbated in HepG2 cells that internalized these endosomes (Fig. 3*C* and *D*). There was no significant difference in endocytosis or lipid accumulation in HepG2 cells after incubation with exosomes from either si*Ctr*- or si*Prkaα1*-treated adipocytes without the PA pretreatment (Fig. 3*A*–*D*). Importantly, incubating HepG2 cells with PA-pretreated si*Ctr* exosomes increased interleukin-6 (IL-6) and MCP-1 levels, and this effect was augmented with si*Prkaα1* exosomes (Fig. 3*E*–*I*). Meanwhile, cleaved caspase-3 levels also increased in HepG2 cells after incubation with PA-pretreated si*Ctr* exosomes. Again, the effect in HepG2 cells was amplified after incubation with si*Prkaα1* exosomes derived from PA pretreated adipocytes (Fig. 3*G* and *J*). These results were verified with immunostaining for cleaved caspase-3 (Fig. 3*K* and *L*). Collectively, these data indicate that exosomes derived from PA-pretreated si*Prkaα1*-deficient adipocytes exacerbate HepG2 cell damage.

PA Treatment Increases CD36 Sorting Into Adipocyte-Derived Exosomes

Next, we investigated whether the protein content of the exosomes derived from PA-treated adipocytes affected exosome internalization. Using a nontargeted proteomic profiling MS system, we found that CD36, a lipid transport receptor, was expressed in higher amounts in the exosomes derived from PA-treated adipocytes (Fig. 4*A*). To verify our results, we used Western blotting to probe CD36 expression in exosomes derived from PA-treated WT or *Prkaα1*$^{-/-}$ WATs. Interestingly, WT and *Prkaα1*$^{-/-}$ exosomes did not exhibit increased CD36 levels when quantifying WATs. However, CD36 protein levels were significantly higher in exosomes from PA-pretreated WT and *Prkaα1*$^{-/-}$ cells when compared with cells that were not treated with PA (Fig. 4*B* and *C*). The highest expression of CD36 was detected in exosomes derived from PA-pretreated *Prkaα1*$^{-/-}$ adipocytes. Increased CD63 and CD81 protein levels were detected in exosomes derived from *Prkaα1*$^{-/-}$, PA-treated WT, and PA-treated *Prkaα1*$^{-/-}$ WATs (Fig. 4*B*–*E*). These results suggest that PA treatment increases CD36 sorting into exosomes.

TSG101 Facilitates CD36 Sorting Into Exosomes

To explore the mechanism of CD36 sorting into exosomes, we measured the expression of CD36 in PA-treated WT and *Prkaα1*$^{-/-}$ WATs. Consistent with a previous report (34), PA treatment significantly increased CD36 protein and mRNA levels in WT and *Prkaα1*$^{-/-}$ WATs (Fig. 4*F*–*H*). It is important to note that AMPKα1 deficiency alone did not change CD36 mRNA and protein expression in WAT. Next, we explored how CD36 is packaged into the exosomes derived from PA-treated adipocytes. Immunoprecipitation indicated that CD36 is associated with TSG101 in both the cytosol and exosomes (Fig. 4*I*). Furthermore, CD36 protein was absent from endosomes after *Tsg101* silencing (Fig. 4*J* and *K*). Taken together, our results suggest that TSG101 binds to CD36 and recruits CD36 into exosomes.

CD36 Silencing Does Not Affect Exosome Secretion but Decreases Exosome Internalization and HepG2 Damage

To determine whether CD36 was involved in exosome biogenesis, *Cd36* expression was knocked down in adipocytes that were transfected with si*Ctr* or si*Prkaα1*$^{-/-}$. *Cd36* silencing did not change either total exosome numbers or cytosol TSG101 protein levels in si*Ctr* or si*Prkaα1*$^{-/-}$ adipocytes (Supplementary Fig. 6*A*–*D*). Although CD36 silencing significantly reduced exosomal CD36 protein content, it did not affect CD63 expression in exosomes (Supplementary Fig. 6*E*–*G*), indicating that *Cd36* silencing does not affect exosome secretion in adipocytes.

Next, we investigated if CD36 in exosomes mediated lipid uptake and HepG2 cell damage. HepG2 cells were treated with equal numbers of exosomes isolated from adipocytes that were transfected with si*Ctr* and si*Cd36*. As illustrated in Fig. 5*A* and *B*, these experiments revealed a significant decrease in the endocytosis of exosomes derived from *Cd36*-knockdown adipocytes. Adipocyte pretreatment with PA did not have a pronounced effect on exosome uptake by HepG2 cells. In agreement with the observed endocytosis patterns, the exosomes derived from the *Cd36*-knockdown adipocytes were associated with decreased lipid accumulation (Fig. 5*C* and *D*) and apoptosis in HepG2 cells (Fig. 5*E* and *F*). These data suggest that the presence of CD36 augments exosome endocytosis, lipid accumulation, and apoptosis in HepG2 cells.

WAT-Specific AMPKα1 Deletion Enhances HFD-Induced Exosome Release in Serum and WAT

To determine the role of AMPKα1 in exosome secretion from WAT in vivo, we isolated exosomes from the serum and WAT of HFD-fed *Prkaα1*$^{-/-}$, *Prkaα1*$^{fl/fl}$, *Prkaα1*$^{fl/fl}$:*Adipo*$^{Cre+}$, and *Prkaα1*$^{fl/fl}$:*Alb*$^{Cre+}$ mice. The HFD treatment significantly increased serum exosome numbers in *Prkaα1*$^{-/-}$ and *Prkaα1*$^{fl/fl}$:*Adipo*$^{Cre+}$ mice, but not in *Prkaα1*$^{fl/fl}$:*Alb*$^{Cre+}$ and *Prkaα1*$^{fl/fl}$ mice (Fig. 6*A*). In addition, CD63 expression increased in the exosomes isolated from *Prkaα1*$^{-/-}$ and *Prkaα1*$^{fl/fl}$:*Adipo*$^{Cre+}$ mice when compared with the *Prkaα1*$^{fl/fl}$:*Alb*$^{Cre+}$ and *Prkaα1*$^{fl/fl}$ mice (Fig. 6*B*). Similarly, PA treatment increased exosome numbers and CD63 protein levels in *Prkaα1*$^{-/-}$ and *Prkaα1*$^{fl/fl}$:*Adipo*$^{Cre+}$ WATs, but not in *Prkaα1*$^{fl/fl}$:*Alb*$^{Cre+}$ and *Prkaα1*$^{fl/fl}$ WATs (Fig. 6*C* and *D*). These results indicate that an AMPKα1 deficiency in WAT enhances HFD-induced exosome release in serum and WAT.

Absence of AMPKα1 in WAT Exacerbates an HFD-Induced Fatty Liver

To evaluate if WAT derived-exosomes were involved in an HFD-induced fatty liver, we fed *Prkaα1*$^{fl/fl}$, *Prkaα1*$^{-/-}$,

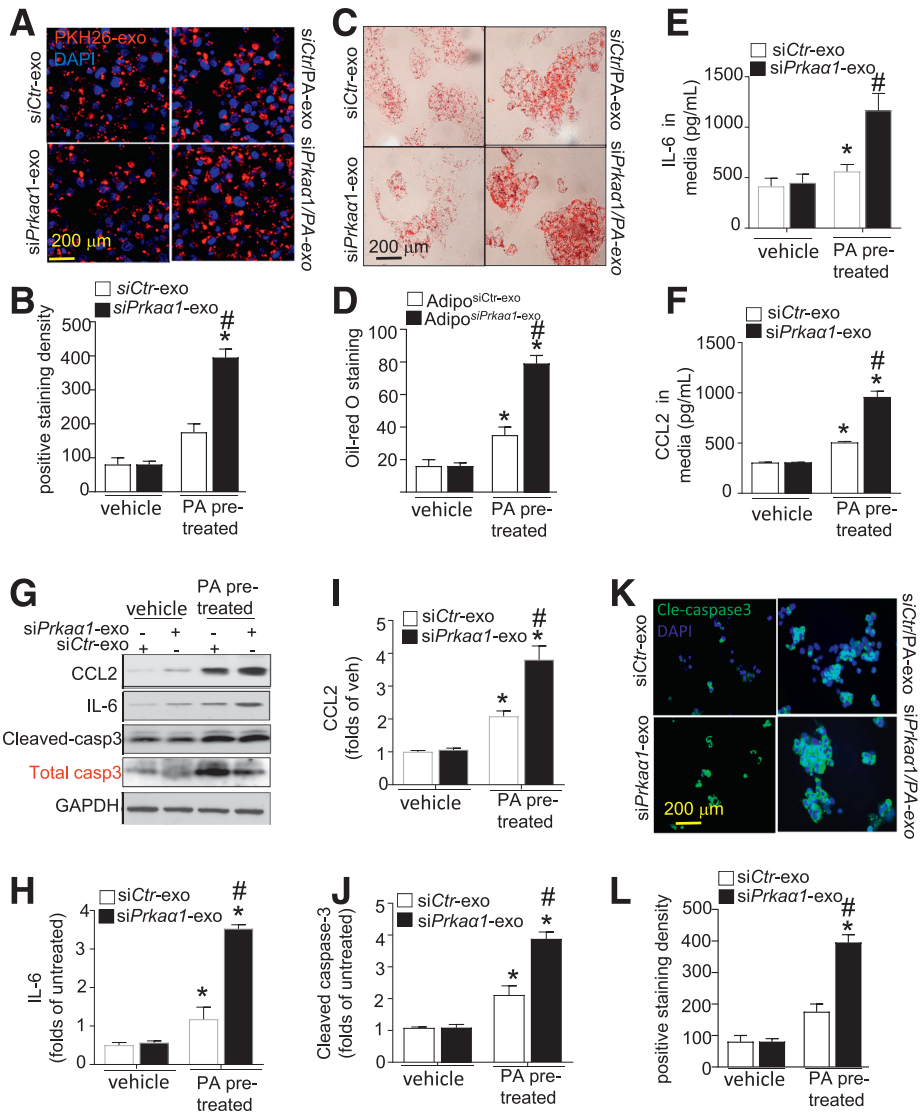

Figure 3—AMPKα1 downregulation exacerbates HepG2 cell damage induced by exosomes derived from PA-treated adipocytes. HepG2 cells were treated with exosomes (exo) derived from adipocytes (Adipo) that were pretreated with or without PA and transfected with *siCtr or siPrkraα1*. *A*: Immunofluorescence analysis of HepG2 cells that internalized PKH26-labeled exosomes. *B*: Quantitative analysis of exosome internalization by HepG2 cells. *C*: Representative images of Oil Red O staining. *D*: Quantification of Oil Red O staining. ELISA for IL-6 (*E*) and CCL2 (*F*) in the supernatant of HepG2 cells. *G*: Western blot for IL-6, CCL2, total caspase-3 (casp3), and cleaved caspase-3 in HepG2 cells. *H–J*: Densitometric analysis of Western blots for IL-6, CCL2, and cleaved caspase-3. *K*: Immunostaining for cleaved caspase-3 (Cle-caspase3) in HepG2 cells. *L*: Quantification of cleaved caspase-3 staining. *$P < 0.05$ vs. control; #$P < 0.05$ vs. vehicle group ($n = 3$). si*Ctr*-exo, exosome derived from adipocytes transfected with control siRNA; si*Ctr*/PA-exo, exosome derived from adipocytes transfected with control siRNA and pretreated with PA; *siPkraα1*-exo, exosome derived from adipocytes transfected with *Pkraa1* siRNA; *siPkraα1*/PA-exo, exosome derived from adipocytes transfected with *Pkraa1* siRNA and pretreated with PA.

Prkaα1$^{fl/fl}$:*Adipo*$^{Cre+}$, and *Prkaα1*$^{fl/fl}$:*Alb*$^{Cre+}$ mice an HFD for 3 months. An HFD had a greater effect on increased overall mouse body weight (Fig. 6*E*), the amount of weight gained (Fig. 6*F*), increased liver weight (Fig. 6*G*), and the ratio of liver weight to body weight (Fig. 6*H*) in *Prkaα1*$^{-/-}$ and *Prkaa1*$^{fl/fl}$:*Adipo*$^{Cre+}$ mice when compared with *Prkaα1*$^{fl/fl}$ and *Prkaa1*$^{fl/fl}$:*Alb*$^{Cre+}$ mice. In addition, serum and hepatic triglycerides (Fig. 6*H*), cholesterol (Fig. 6*H*), AST, ALT, and inflammatory factors tumor necrosis factor-α and IL-6 levels (Supplementary Fig. 7) were higher in *Prkaa1*$^{-/-}$ and *Prkaa1*$^{fl/fl}$:*Adipo*$^{Cre+}$ mice when compared with *Prkaa1*$^{fl/fl}$ and *Prkaa1*$^{fl/fl}$:*Alb*$^{Cre+}$ mice (Fig. 6*I–L*). The elevated lipid accumulation and fatty liver development in *Prkaa1*$^{-/-}$ and *Prkaa1*$^{fl/fl}$:*Adipo*$^{Cre+}$ mice were verified by Oil Red O and H&E staining (Fig. 6*M*). These results confirm that an AMPKα1 deficiency in ATs aggravates HFD-induced liver impairment.

Metformin Inhibits an HFD-Induced Fatty Liver and Exosome Secretion by Activating AMPKα1 in WAT

To address if AMPKα1 activation mitigated HFD-induced liver impairment by reducing exosome secretion in vivo,

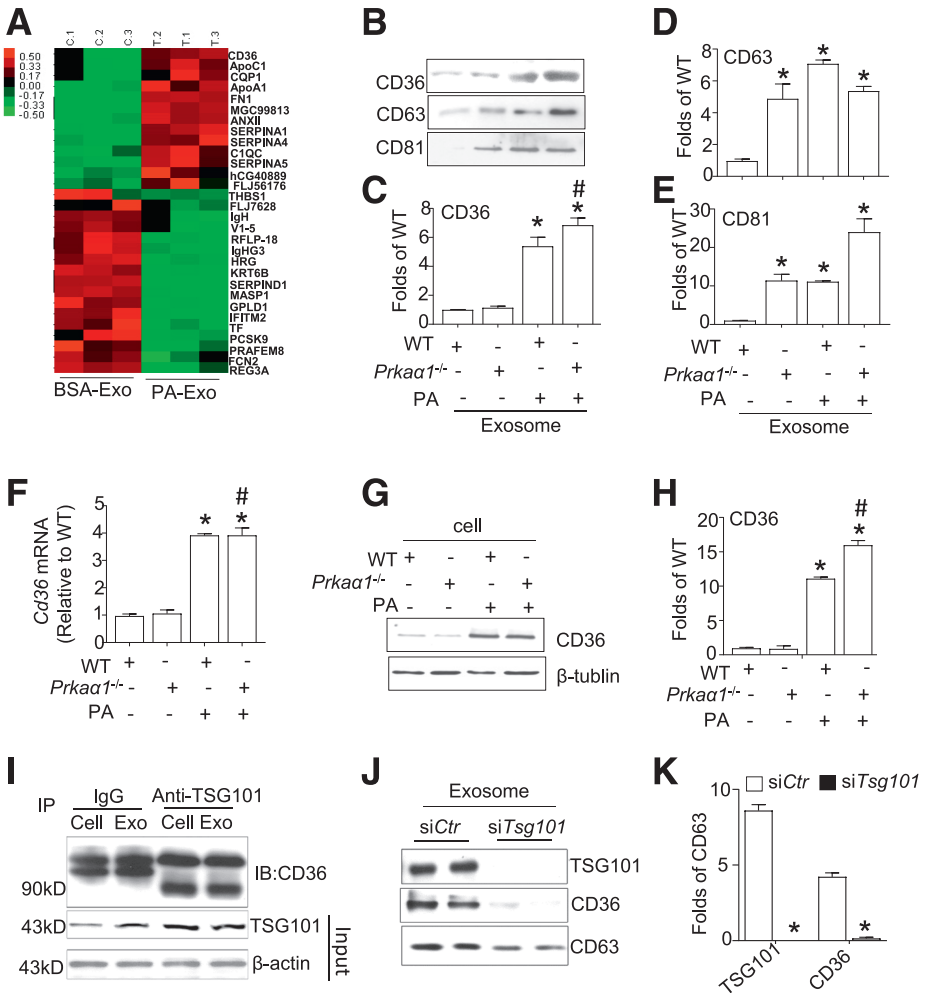

Figure 4—TSG101 facilitates CD36 sorting into exosomes in PA-treated adipocytes. *A*: Proteomic analysis of exosomes derived from adipocytes treated with or without PA. *B*: Western blot for CD36, CD63, and CD81 in exosomes from PA-treated (300 μmol/L) WT and *Prkaα1*$^{-/-}$ WAT. *C*–*E*: Densitometric analysis of CD36, CD63, and CD81 Western blots from *B*. *F*: Expression of Cd36 mRNA in PA-treated WT and *Prkaα1*$^{-/-}$ WAT. *G*: Western blot for CD36 in PA-treated WT and *Prkaα1*$^{-/-}$ WAT. *H*: Densitometric analysis of Western blots for CD36 from *G*. *I*: IP assay for the interaction between TSG101 and CD36 in the cytosol and exosome (Exo) lysates. *J*: Western blot for CD36 in 3T3L1 cells transfected with or without *Tsg101*. *K*: Quantitative data for TSG101. *$P < 0.05$ vs. control ($n = 3$); #$P < 0.05$ vs. PA-treated group ($n = 3$). IB, immunoblotting.

we treated *Prkaa1*$^{fl/fl}$, *Prkaa1*$^{-/-}$, *Prkaa1*$^{fl/fl}$:*Adipo*$^{Cre+}$, and *Prkaa1*$^{fl/fl}$:*Alb*$^{Cre+}$ mice with an HFD and metformin (5 mg/kg/day in drinking water) (35) for 3 months. Metformin administration significantly ameliorated lipid accumulation (Supplementary Fig. 8*A* and *B*), liver weight (Supplementary Fig. 8*C*), and the ratio of liver weight to body weight (Supplementary Fig. 8*D*) in *Prkaa1*$^{fl/fl}$ *and Prkaa1*$^{fl/fl}$:*Alb*$^{Cre+}$ mice. However, metformin treatment failed to mitigate an HFD-induced fatty liver in *Prkaa1*$^{-/-}$ and *Prkaa1*$^{fl/fl}$:*Adipo*$^{Cre+}$ mice. Notably, metformin significantly reduced HFD-induced exosome release into serum and WAT in *Prkaa1*$^{fl/fl}$:*Alb*$^{Cre+}$ and *Prkaa1*$^{fl/fl}$ mice, but not in *Prkaa1*$^{-/-}$ and *Prkaa1*$^{fl/fl}$:*Adipo*$^{Cre+}$ mice (Supplementary Fig. 8*E* and *F*). These results indicate that metformin mitigates HFD-induced liver impairment or inhibits exosome shedding by specific activation of AMPKα1 in WAT in vivo.

Blocking Exosome Shedding Ablates HFD-Induced NAFL

To validate that exosome shedding aggravated fatty liver development induced by an AMPKα1 deficiency in vivo, we inhibited exosome secretion with intraperitoneal injections of GW4869 (0.5 mg/kg/day) in HFD-fed *Prkaa1*$^{-/-}$ and *Prkaa1*$^{fl/fl}$:*Adipo*$^{Cre+}$ mice for 8 weeks. GW4869 is a ceramide-induced exosome inhibitor (32). Consistent with its known function, GW4869 administration significantly reduced exosome secretion from WAT (Fig. 7*A*) and was associated with decreased liver weights (Fig. 7*B*) and liver weight to body weight ratios (Fig. 7*C*) in all four HFD-fed strains of mice. Importantly, Oil Red O and H&E staining revealed that GW4869 treatment attenuated lipid accumulation and fatty liver development in both *Prkaa1*$^{-/-}$ and *Prkaa1*$^{fl/fl}$:*Adipo*$^{Cre+}$ mice (Fig. 7*D*–*F*). In summary, our results support the framework that

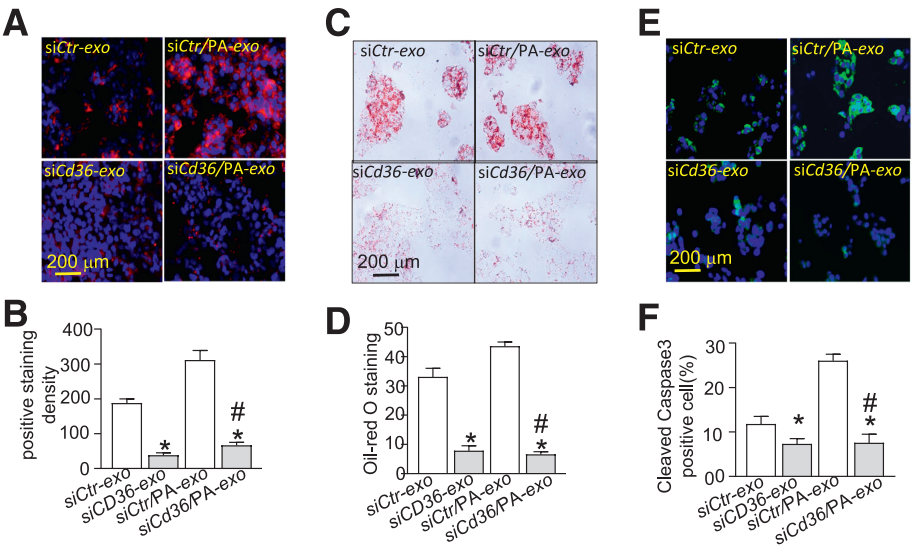

Figure 5— Silencing CD36 attenuates exosome internalization and HepG2 damage. *A*: HepG2 cells were treated with exosomes (exo) derived from adipocytes that were transfected with *siCtr or siCd36* and treated with or without PA. *B*: Quantitative analysis of exosome internalization by HepG2 cells. *C*: Representative images of Oil Red O staining in HepG2 cells treated by exosomes derived from adipocytes that were transfected with *siCtr or siCd36* and treated with or without PA. *D*: Quantification of Oil Red O staining. *E*: Immunostaining for cleaved caspase-3 in HepG2 cells treated by exosomes derived from adipocytes that were transfected with *siCtr or siCd36* and treated with or without PA. *F*: Quantification of cleaved caspase-3 staining. *siCD36-exo*, exosome derived from adipocytes transfected with si*Cd36*; *siCd36*/PA-*exo*, exosome derived from adipocytes transfected with si*Cd36* and pretreated with PA; *siCtr-exo*, exosome derived from adipocytes transfected with si*Control*; *siCtr*/PA-*exo*, exosome derived from adipocytes transfected with si*Control* and pretreated with PA. *$P < 0.05$ vs. *siCtr*-exo group ($n = 3$); #$P < 0.05$ vs. *siCtr*/PA-exo group ($n = 3$).

inhibiting exosome secretion from WAT prevents an HFD-induced fatty liver.

DISCUSSION

In this study, we have demonstrated that AMPKα1 is a critical molecule that regulates exosome synthesis, content, and shedding in WAT. Inactivation of AMPKα1 in WAT increased exosome release and mediated the development of an NAFL. Furthermore, AMPKα1 knockdown increased exosome shedding and promoted CD36 accumulation in exosomes that were derived from adipocytes treated with PA. Collectively, the effects of AMPKα1 knockdown mediated PA-induced hepatocyte damage. We also found that an HFD induced more severe liver damage in *Prkaa1*$^{-/-}$ and AT-specific *Prkaa1*$^{-/-}$ mice. Activation of AMPK by metformin reduced exosome release and contributed to a fatty liver in WT and liver-specific *Prkaa1*$^{-/-}$ mice. Inhibiting exosome secretion with GW4869 alleviated an HFD-induced fatty liver in *Prkaa1*$^{-/-}$ and adipocyte-specific *Prkaa1*$^{-/-}$ mice. Our study suggests that inhibition of exosome release from WAT is a novel therapeutic target for treating NAFLD (Supplementary Fig. 9).

The most important finding of our study was that AMPKα1 inhibition in WAT contributed to an NAFL caused by an HFD through increased exosome numbers and CD36 protein content. We observed exosomes derived from WT or AMPKα1-deficient adipocytes did not induce significant hepatocyte damage. However, after the addition of an adipocyte PA pretreatment, the uptake of exosomes derived from AMPKα1-deficient adipocytes was increased and damaging to hepatocytes. These data suggest that exosomes derived from PA-treated adipocytes are different and that these differences have detrimental effects on liver structure and function. Consistent with this hypothesis, we found that an AMPKα1-specific deficiency in WAT, but not in the liver, aggravated an HFD-induced NAFL. The AMPKα1-specific knockdown in WAT was accompanied by increased exosomes in both serum and WAT. Moreover, GW4869, but not metformin, dramatically mitigated fatty liver development in *Prkaa1*$^{fl/fl}$:*Adipo*$^{Cre+}$ mice.

The following evidence supports our conclusion: first, in adipocytes, activation of AMPK inhibited PA-induced exosome secretion, and conversely, repression of AMPK enhanced exosome secretion. Second, the absence of AMPKα1, but not the AMPKα2 isoform, increased exosome secretion in WAT. Third, AMPKα1 knockdown in adipocytes enhanced exosome secretion due to increased microvesicle biogenesis mediated by elevated TSG101 expression. Finally, repression of AMPKα1 led to elevated TSG101 protein levels, but had no effect on mRNA expression, which indicated that AMPKα1 may regulate TSG101 degradation. Taken together, these results strongly support the hypothesis that decreased AMPKα1 levels instigate lipid deposition in the liver through TSG101-mediated exosome biogenesis.

We have elucidated the mechanisms by which AMPKα1 downregulation affects exosomal contents and induces

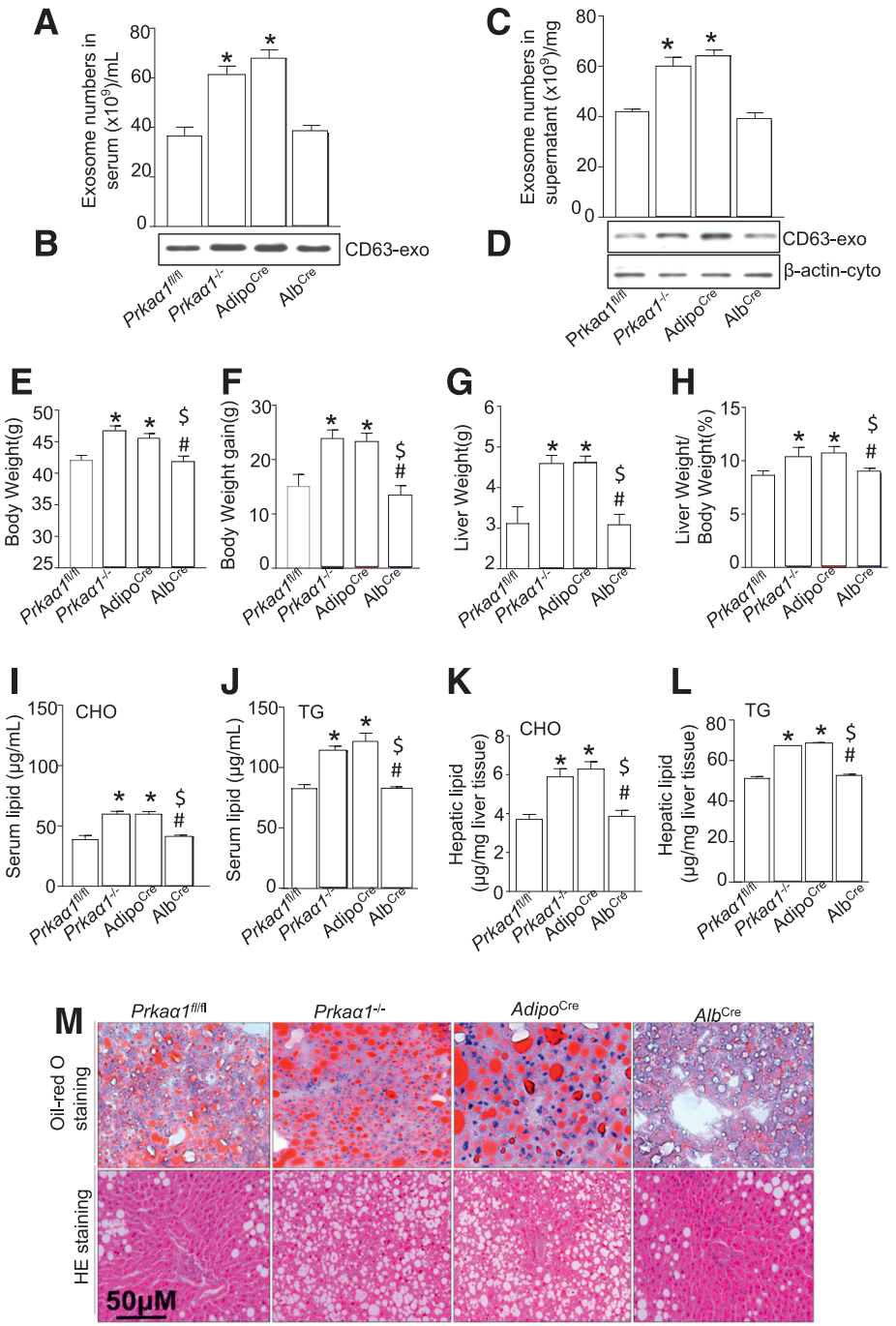

Figure 6—AMPKα1 deficiency increases HFD-enhanced exosome shedding from WAT and exacerbates lipid accumulation in the liver. *A*: Quantification of serum exosomes (exo) in *Prkaα1*$^{fl/fl}$, *Prkaα1*$^{-/-}$, *Adipo*^{Cre}, and *Alb*^{Cre} mice fed an HFD for 3 months ($n = 4$ for each group). *B*: Western blot for CD63 in the exosomes from *A*. *C*: Quantification of exosomes in the supernatant of *Prkaα1*$^{fl/fl}$, *Prkaα1*$^{-/-}$, *Adipo*^{Cre}, and *Alb*^{Cre} WAT. *D*: Western blot for CD63 in the exosomes from *C*. *E–M*: *Prkaα1*$^{fl/fl}$, *Prkaα1*$^{-/-}$, *Adipo*^{Cre}, and *Alb*^{Cre} mice were fed an HFD for 3 months. *E*: Body weight. *F*: Increase in body weight. *G*: Liver weight. *H*: Ratio of liver weight to body weight. *I*: Serum cholesterol (CHO) levels. *J*: Serum triglyceride (TG) levels. *K*: Hepatic CHO levels. *L*: Hepatic TG levels. *M*: Representative images of Oil Red O and H&E (HE) staining of the liver tissues. *$P < 0.05$ vs. *Prkaα1*$^{fl/fl}$ mice; #$P < 0.05$ vs. *Prkaα1*$^{-/-}$ mice ($n = 3$); \$$P < 0.05$ vs. *Adipo*^{Cre} *mice* ($n = 3$). *Adipo*^{Cre}, *Prkaα1*$^{fl/fl}$*:Adipo*^{Cre} *mice*; *Alb*^{Cre}, *Prkaα1*$^{fl/fl}$*:Alb*^{Cre} *mice.*

HepG2 cell damage under PA stimulation. A nontargeted proteomic profiling MS array revealed there were 43 different proteins in the exosomes derived from PA-treated adipocytes. Among the exosomal proteins, CD36 was the most abundant. Importantly, CD36 mediates lipid uptake in vitro and in vivo. CD36 silencing has previously been found to attenuate lipid accumulation in liver tissue (36). Therefore, we explored the role of CD36 NAFL development

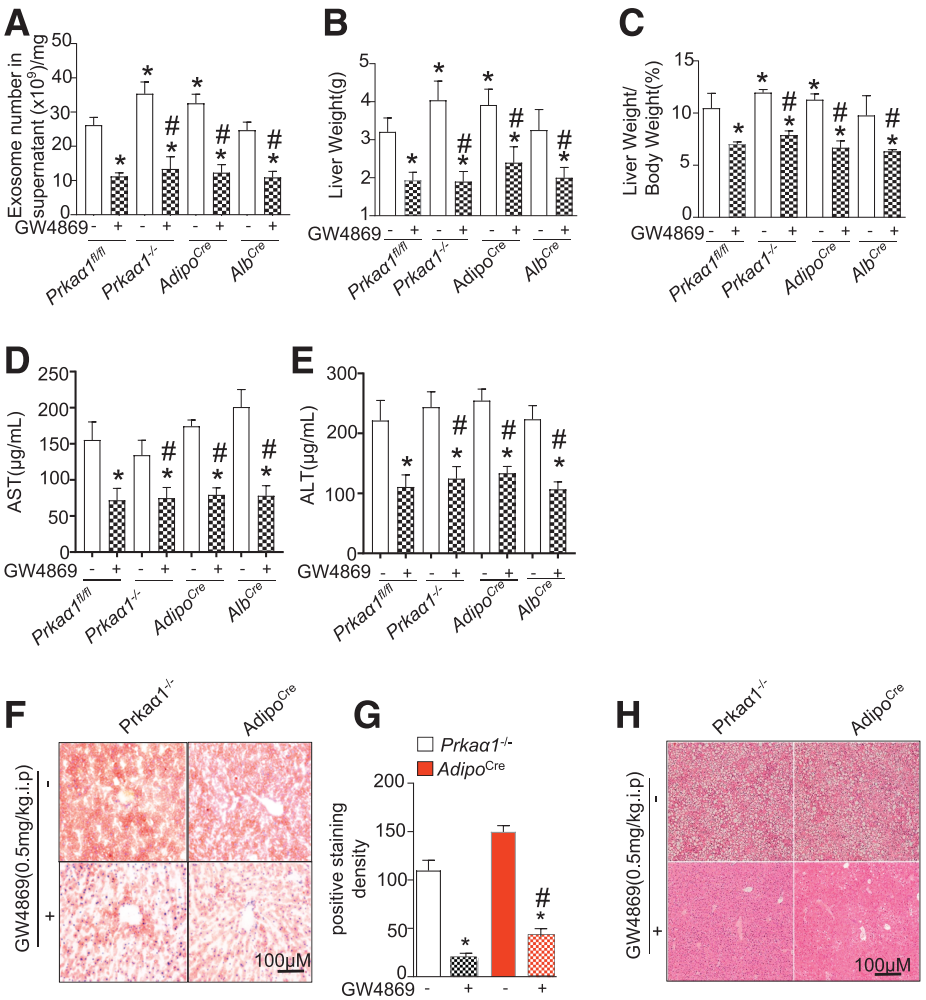

Figure 7—Inhibition of exosome release from WAT mitigates an HFD-induced fatty liver. *Prkaα1*$^{fl/fl}$, *Prkaα1*$^{-/-}$, *Adipo*^{Cre}, and *Alb*^{Cre} mice were fed an HFD and GW4869 (0.5 mg/kg/day, i.p.) for 3 months. *A*: Quantification of exosomes in the supernatant. *B*: Liver weight. *C*: Ratio of liver weight to body weight. *D*: AST. *E*: ALT. *F*: Representative images of Oil Red O staining. *G*: Quantification of Oil Red O staining ($n = 6$). *H*: Representative images of H&E staining. *$P < 0.05$ vs. *Prkaα1*$^{fl/fl}$ mice; #$P < 0.05$ vs. every group of mice treated with vehicle. *Adipo*^{Cre}, *Prkaα1*$^{fl/fl}$*:Adipo*^{Cre} *mice*; *Alb*^{Cre}, *Prkaα1*$^{fl/fl}$*:Alb*^{Cre} *mice.*

by investigating exosome secretion in adipocytes after CD36 silencing. Interestingly, *Cd36* silencing did not affect exosome secretion; however, exosome internalization by hepatocytes and hepatocyte damage were significantly mitigated. These data suggest that CD36 is a primary mediator of fatty liver development due to its high expression in obesity and HFD-treated adipocytes. In addition, an AMPKα1 deficiency increased TSG101 expression and promoted CD36 to sort into exosomes.

Our results indicate that AMPK activators, such as metformin, might have therapeutic effects on NAFLD. No studies have evaluated whether metformin improves long-term patient-oriented outcomes, such as progression from NAFLD to nonalcoholic steatohepatitis, cirrhosis, hepatocellular carcinoma, or death from liver failure. Rather, a considerable body of evidence on the hepatic effects of metformin have yielded mixed results, indicating there is potentially modest benefit that has yet to be confirmed due to the small sample sizes and short terms of the studies and inconsistently reported outcomes (37–41). NAFLD is intricately linked to insulin resistance and its associated metabolic features (e.g., higher body weight, BMI, and waist circumference), so by improving metabolic features of NAFLD, metformin could also improve management of this liver disease. Indeed, a systematic review by Li et al. (42) demonstrated that metformin can improve biochemical and metabolic features in NAFLD. Larger randomized controlled trials of sufficient duration that use histological end points are needed to assess the effectiveness of this drug in modifying the progression of NAFLD.

In summary, our results demonstrate that AMPKα1 downregulation contributes to an HFD-induced NAFL.

AMPKα1 downregulation enhances the communication between WAT and the liver via increased exosome biogenesis and secretion. Inhibiting exosome release from WAT by AMPK activation is a novel therapeutic target for treating NAFL development.

Funding. This study was supported by the National Natural Science Foundation of China (grants 81670276 to Y.H. and 82070300 to C.Y.). This study was also supported in part by the National Institutes of Health grants HL079584, HL080-499, HL089920, and HL110488 (to M.-H.Z.).

Duality of Interest. No potential conflicts of interest relevant to this article were reported.

Author Contributions. M.-H.Z. conceived the project. C.Y. and M.-H.Z. designed the study and wrote the manuscript. X.T., J.L., and D.L. conducted confocal microscopy imaging, IP, and Western blotting. D.Y. conducted site-directed mutagenesis. C.Y. and Z.X. wrote the manuscript. All authors approved the manuscript. C.Y. is the guarantor of this work and, as such, had full access to all of the data in the study and takes responsibility for the integrity of the data and the accuracy of the data analysis.

References

1. Pegtel DM, Gould SJ. Exosomes. Annu Rev Biochem 2019;88:487–514
2. Nazari-Shafti TZ, Emmert MY. The link between exosomes phenotype and mode of action in the context of cardioprotection. Eur Heart J 2019;40:3361
3. LeBleu VS, Kalluri R. Exosomes exercise inhibition of anti-tumor immunity during chemotherapy. Immunity 2019;50:547–549
4. Gao L, Wang L, Dai T, et al. Tumor-derived exosomes antagonize innate antiviral immunity. Nat Immunol 2018;19:233–245
5. Ying W, Riopel M, Bandyopadhyay G, et al. Adipose tissue macrophage-derived exosomal miRNAs can modulate in vivo and in vitro insulin sensitivity. Cell 2017;171:372–384.e12
6. Chen Y, Pfeifer A. Brown fat-derived exosomes: small vesicles with big impact. Cell Metab 2017;25:759–760
7. Thomou T, Mori MA, Dreyfuss JM, et al. Adipose-derived circulating miRNAs regulate gene expression in other tissues. Nature 2017;542:450–455
8. Sciorati C, Clementi E, Manfredi AA, Rovere-Querini P. Fat deposition and accumulation in the damaged and inflamed skeletal muscle: cellular and molecular players. Cell Mol Life Sci 2015;72:2135–2156
9. Furman D, Campisi J, Verdin E, et al. Chronic inflammation in the etiology of disease across the life span. Nat Med 2019;25:1822–1832
10. Sanyal AJ. Past, present and future perspectives in nonalcoholic fatty liver disease. Nat Rev Gastroenterol Hepatol 2019;16:377–386
11. Ji C, Guo X. The clinical potential of circulating microRNAs in obesity. Nat Rev Endocrinol 2019;15:731–743
12. Crewe C, Joffin N, Rutkowski JM, et al. An endothelial-to-adipocyte extracellular vesicle axis governed by metabolic state. Cell 2018;175:695–708.e13
13. Kita S, Maeda N, Shimomura I. Interorgan communication by exosomes, adipose tissue, and adiponectin in metabolic syndrome. J Clin Invest 2019;129:4041–4049
14. Akbar N, Azzimato V, Choudhury RP, Aouadi M. Extracellular vesicles in metabolic disease. Diabetologia 2019;62:2179–2187
15. Zou W, Lai M, Zhang Y, et al. Exosome release is regulated by mTORC1. Adv Sci (Weinh) 2018;6:1801313
16. Sato K, Meng F, Glaser S, Alpini G. Exosomes in liver pathology. J Hepatol 2016;65:213–221
17. Foretz M, Guigas B, Viollet B. Understanding the glucoregulatory mechanisms of metformin in type 2 diabetes mellitus. Nat Rev Endocrinol 2019;15:569–589
18. Jordan S, Tung N, Casanova-Acebes M, et al. Dietary intake regulates the circulating inflammatory monocyte pool. Cell 2019;178:1102–1114.e17
19. Steinberg GR, Carling D. AMP-activated protein kinase: the current landscape for drug development. Nat Rev Drug Discov 2019;18:527–551
20. Patra KC, Weerasekara VK, Bardeesy N. AMPK-mediated lysosome biogenesis in lung cancer growth. Cell Metab 2019;29:238–240
21. Foretz M, Guigas B, Bertrand L, Pollak M, Viollet B. Metformin: from mechanisms of action to therapies. Cell Metab 2014;20:953–966
22. Hardie DG. AMPK–sensing energy while talking to other signaling pathways. Cell Metab 2014;20:939–952
23. Mizunoe Y, Sudo Y, Okita N, et al. Involvement of lysosomal dysfunction in autophagosome accumulation and early pathologies in adipose tissue of obese mice. Autophagy 2017;13:642–653
24. Wang B, Nie J, Wu L, et al. AMPKα2 protects against the development of heart failure by enhancing mitophagy via PINK1 phosphorylation. Circ Res 2018;122:712–729
25. Wang Q, Wu S, Zhu H, et al. Deletion of PRKAA triggers mitochondrial fission by inhibiting the autophagy-dependent degradation of DNM1L. Autophagy 2017;13:404–422
26. Liu Z, Zhu H, Dai X, et al. Macrophage liver kinase B1 inhibits foam cell formation and atherosclerosis. Circ Res 2017;121:1047–1057
27. Lorente-Cebrián S, Bustos M, Marti A, Martinez JA, Moreno-Aliaga MJ. Eicosapentaenoic acid stimulates AMP-activated protein kinase and increases visfatin secretion in cultured murine adipocytes. Clin Sci (Lond) 2009;117:243–249
28. Ban LA, Shackel NA, McLennan SV. Extracellular vesicles: a new frontier in biomarker discovery for non-alcoholic fatty liver disease. Int J Mol Sci 2016;17:376
29. Sahoo S, Losordo DW. Exosomes and cardiac repair after myocardial infarction. Circ Res 2014;114:333–344
30. Roche JV, Nesverova V, Olsson C, Deen PM, Törnroth-Horsefield S. Structural insights into AQP2 targeting to multivesicular bodies. Int J Mol Sci 2019;20:5351
31. Bänfer S, Schneider D, Dewes J, et al. Molecular mechanism to recruit galectin-3 into multivesicular bodies for polarized exosomal secretion. Proc Natl Acad Sci U S A 2018;115:E4396–E4405
32. Wang Y, Jia L, Xie Y, et al. Involvement of macrophage-derived exosomes in abdominal aortic aneurysms development. Atherosclerosis 2019;289:64–72
33. Colombo M, Moita C, van Niel G, et al. Analysis of ESCRT functions in exosome biogenesis, composition and secretion highlights the heterogeneity of extracellular vesicles. J Cell Sci 2013;126:5553–5565
34. Costantino S, Akhmedov A, Melina G, et al. Obesity-induced activation of JunD promotes myocardial lipid accumulation and metabolic cardiomyopathy. Eur Heart J 2019;40:997–1008
35. Miller RA, Chu Q, Xie J, Foretz M, Viollet B, Birnbaum MJ. Biguanides suppress hepatic glucagon signalling by decreasing production of cyclic AMP. Nature 2013;494:256–260
36. Zhao L, Zhang C, Luo X, et al. CD36 palmitoylation disrupts free fatty acid metabolism and promotes tissue inflammation in non-alcoholic steatohepatitis. J Hepatol 2018;69:705–717
37. Pan CS, Stanley TL. Effect of weight loss medications on hepatic steatosis and steatohepatitis: a systematic review. Front Endocrinol (Lausanne) 2020;11:70
38. Fan H, Pan Q, Xu Y, Yang X. Exenatide improves type 2 diabetes concomitant with non-alcoholic fatty liver disease. Arq Bras Endocrinol Metabol 2013;57:702–708
39. Feng W, Gao C, Bi Y, et al. Randomized trial comparing the effects of gliclazide, liraglutide, and metformin on diabetes with non-alcoholic fatty liver disease. J Diabetes 2017;9:800–809
40. Garinis GA, Fruci B, Mazza A, et al. Metformin versus dietary treatment in nonalcoholic hepatic steatosis: a randomized study. Int J Obes 2010;34:1255–1264
41. Handzlik G, Holecki M, Kozaczka J, et al. Evaluation of metformin therapy using controlled attenuation parameter and transient elastography in patients with non-alcoholic fatty liver disease. Pharmacol Rep 2019;71:183–188
42. Li Y, Liu L, Wang B, Wang J, Chen D. Metformin in non-alcoholic fatty liver disease: a systematic review and meta-analysis. Biomed Rep 2013;1:57–64